Strong Destabilization of Stable Modes with a Half-Frequency Associated with Chirping Geodesic Acoustic Modes in the Large Helical Device

Observation of strong destabilization of stable modes with a half frequency associated with chirping EGAMs in the LHD

T. Ido[1,*], K. Itoh[1], M. Osakabe[1,4], M. Lesur[2], A. Shimizu[1], K. Ogawa[1,4], K. Toi[1], M. Nishiura[3], S. Kato[1], M. Sasaki[2], K. Ida[1,4], S. Inagaki[2], S.–I. Itoh[2], and the LHD Experiment Group[1]

[1]*National Institute for Fusion Science, 322-6 Oroshi, Toki, Gifu 509-5292, Japan*

[2]*Research Institute for Applied Mechanics, Kyushu University, 6-1 Kasuga-koen, Kasuga, Fukuoka, 816-8580, Japan*

[3]*Graduate School of Frontier Sciences, University of Tokyo, 5-1-5 Kashiwanohara, Kashiwa, Chiba, 277-8561, Japan*

[4]*SOKENDAI (The Graduate University for Advanced Study), 322-6 Oroshi, Toki, Gifu 509-5292, Japan*

Abrupt and strong excitation of a mode has been observed when the frequency of chirping energetic-particle driven geodesic acoustic mode (EGAM) reaches twice the GAM frequency. The frequency of the secondary mode is the GAM frequency, which is a half frequency of the primary EGAM. Based on analysis of spatial structures, the secondary mode is identified as a GAM. The phase relation between the secondary mode and the primary EGAM is locked, and the evolution of the growth rate of the secondary mode indicates the nonlinear excitation. The results suggest that the primary mode (EGAM) contributes to nonlinear destabilization of a subcritical mode.

PACS: 52.35.Mw, 52.35.FP, 52.55.Pi

Particles and heat transport in magnetized fusion plasmas are strongly affected by fluctuations such as microscopic turbulence and energetic particle-driven macroscopic modes. In order to assess the impacts of fluctuations on transport, understanding behaviors, especially the saturation level, of fluctuations in plasmas is essential.

In the past decade, zonal flow excited by nonlinear coupling of turbulence has attracted much attention, as summarized in Ref.[1], because it can spontaneously regulate the saturation level of turbulence. Recent studies have clarified that the geodesic acoustic mode (GAM)[2], which is an oscillatory zonal flow, is excited not only by turbulence[3, 4] but also by energetic particles[5, 6]. The GAM can also affect transport of energetic particles. For example, large neutron emission drops following energetic-particle driven GAM (EGAM) bursts in DIII-D suggest losses of energetic ions[7]. In addition, EGAMs might provide a new channel of energy transfer from energetic fusion products to the thermal plasma [8, 9], or might couple with turbulence and significantly degrade confinement [10]. Therefore, investigation of the GAM is necessary to understand transport of both thermal plasma and energetic particles.

The EGAM is routinely observed in toroidal plasmas, such as JET[11], DIII-D[7], HL-2A[12] and the LHD[13, 14, 15]. It often features frequency chirping on a time scale much faster than the evolution of plasma equilibrium. This phenomenon is attributed to the evolution of structures in the velocity space of the energetic particle distribution, which are formed by resonant wave-particle interactions [16, 5, 17]. In the LHD, we found that a chirping EGAM, with a duration of 10 ms, was sometimes accompanied by abrupt and stronger burst, with one-half the frequency of the EGAM, and with a duration of 1 ms or less, which is much faster than the temporal evolution of the EGAM. In this letter, the chirping EGAM and the abruptly excited mode are called a *primary mode* and a *secondary mode*, respectively, for convenience. Since the secondary mode has lower frequency and larger amplitude than the primary mode, the influence on thermal plasmas may be more significant. In addition, experimental identification of an abrupt excitation of the global secondary mode sheds light on the 'triggering problem' (i.e., the sudden acceleration of the growth rate of large scale deformation in plasmas), which has long been a challenge in laboratory and astro plasmas[18, 19]. In this letter, we identify the secondary mode, and demonstrate the nonlinear coupling between the EGAM and the secondary mode, by analyzing magnetic field fluctuations ($\tilde{B}_\theta$) measured by Mirnov coils, and both electric potential fluctuations ($\tilde{\phi}$) and density fluctuations ($\tilde{n}$) measured by a heavy ion beam probe (HIBP).

The LHD is a heliotron device. In this series of experiments, the magnetic field strength is 1.375 T at the magnetic axis, and the major (R) and averaged minor radii of plasma are 3.75 m and about 0.6 m, respectively. Fueling gas is hydrogen, and the plasmas are produced and sustained by a neutral hydrogen beam injection (NBI). The injected beam energy is 175 keV and the power of the neutral beam ionized in the plasma is about 140 kW. In order to increase the slowing-down time of the beam and to maintain a positive gradient in the velocity space of the beam for strong EGAM excitation, the electron temperature (T_e) is increased by superposing electron cyclotron heating (ECH) with a power of 2.5 MW. Electron

density is kept low in the experiments. In typical discharges, the line averaged electron density is 0.1×10^{19} (m^{-3}), the central T_e is approximately 8 keV, the ion temperature (T_i) is several 100 eV and the slowing-down time of the injected beam ion is approximately 20 s.

The setup of diagnostics is the same as that in Ref.[15]. Six Mirnov coils are installed on the vacuum vessel of the LHD at distant toroidal locations and the toroidal mode structure of $\tilde{B}_\theta$ can be measured. The radial profiles of $\tilde{\phi}$ and $\tilde{n}$ are measured by moving the measurement position of the HIBP at a sweep frequency of 10 Hz from the normalized minor radius of -0.3 to 0.6, where minus and plus mean the lower side and the upper side of the equatorial plane of the torus.

Figure 1 shows a typical waveform of a time derivative of $\tilde{B}_\theta$ ($\dot{B}_\theta$) measured by a Mirnov coil and its spectrogram. Coherent modes with frequency up-chirping from about 50 kHz to 90 kHz appear intermittently (labeled as "EGAM" in the figure). The initial frequency, which is slightly larger than the GAM frequency determined by parameters of the main plasmas ($f_{GAM,b}$), where $f_{GAM,b} = (1/2\pi R)\sqrt{2(T_e + 7T_i/4)/m_i} \sim 42$ kHz and m_i is the ion mass, indicate that the energetic particles contribute significantly to drive the mode, and the mode is identified as EGAM in Ref.[15].

When the frequency of the EGAM reaches around $2f_{GAM,b}$, a secondary mode is abruptly and transiently excited, as marked by white arrows in Fig. 1 (b). The frequency of the secondary mode is $f_{GAM,b}$. The secondary mode appears only when the chirping EGAM presents. Thus, it is normally stable, and the presence of the EGAM is a necessary condition for the secondary mode excitation.

Expanded views of $\tilde{B}_\theta$ and $\tilde{\phi}$ associated with the secondary mode and the EGAM are shown in Fig. 2, for a typical burst. The duration time of the secondary mode is 1 ms or less, and it is much shorter than the duration of the primary EGAM (> 10 ms).

The amplitudes of the secondary mode are about 6 μT for the $\tilde{B}_\theta$ and about 7 kV for $\tilde{\phi}$. They can be almost twice as large as the maximum amplitudes of the primary EGAM, which are about 2.5 μT for the $\tilde{B}_\theta$ and about 4 kV for $\tilde{\phi}$. Although a mode with $3f_{GAM,b}$ is excited as shown in Fig. 2 (a), the amplitude is much smaller than those of the primary and secondary modes. The relation of their amplitudes does not satisfy the Manley-Rowe relation, and it may suggest that the secondary mode is not excited by a simple parametric coupling. In addition, several modes also appear at around 97 kHz, 139 kHz, and 180 kHz. These frequencies correspond to the sum of the higher harmonic frequencies of $f_{GAM,b}(= 41.5\,\text{kHz})$ and 14 kHz. The relation suggests a coupling with the higher harmonics of the $f_{GAM,b}$ mode and a 14 kHz mode. However, their contribution will be negligible in the secondary mode excitation, because their amplitudes are more than two orders of magnitude less than those of the primary mode and the secondary modes. Therefore, only the primary and secondary modes will be mainly described in the following part of this letter.

In order to identify the secondary mode, the spatial structure has been investigated by the Mirnov probe array and the HIBP. The toroidal mode number (n) is zero, because there is no phase delay among $\tilde{B}_\theta$ measured by the Mirnov coils aligned in toroidal direction (Fig. 3).

The radial structures of $\tilde{\phi}$ and $\tilde{n}$ are measured by moving the measurement position of the HIBP. Because the sweep frequency of the probe beam is slower than temporal evolution of the secondary mode, the measurement may include not only spatial structure but also temporal evolution. In order to reduce the influence of the temporal evolution of the modes and changes in the experiment condition, $\tilde{B}_\theta$ measured by a Mirnov coil is used as a reference. This approach is valid because it is confirmed that $\tilde{B}_\theta$ is proportional to $\tilde{\phi}$ for GAM[15]. As shown in Fig. 4 (a), both the primary mode and the secondary mode exist in the central region of the plasma.

Figure 4 (b) and (c) show radial profiles of the phase of $\tilde{\phi}$ and fluctuations of the beam intensity of the HIBP, which reflects $\tilde{n}$. The phase of $\tilde{\phi}$ is symmetric with respect to the equatorial plane of the torus. On the other hand, the phase of $\tilde{n}$ is antisymmetric. The results indicate that the spatial structure of the secondary mode agrees with the dominant structures of the GAM: m = 0 for $\tilde{\phi}$ and m = 1 for $\tilde{n}$, where m is the poloidal mode number. Because the secondary mode has the GAM frequency and the spatial mode structures are consistent with the GAM, it is concluded that the secondary mode is also a GAM.

Let us now focus on the relation between the secondary mode and the primary EGAM. Figure 5 shows Lissajous curves between the Mirnov signals ($\dot{B}_\theta$) associated with the primary mode and the secondary mode, where the signals are normalized by their amplitudes ($|\dot{B}_\theta|$) to extract the phase. The phase relation between the secondary mode and the primary EGAM is locked at 0 - 30 degrees in the growth period and at 90 degrees in the decay period. Such phase relations are reproducible in the other events[20] in other discharges. The observed phase locking clearly indicates a coupling between the primary EGAM and the secondary mode.

The dynamics of the secondary mode excitation is the period doubling event, as shown by trajectories in a phase space. Figure 6 shows the relation between $\dot{B}_\theta$ and $\tilde{B}_\theta$. In the period (A), only a single mode corresponding to the primary mode exists. In the period (B), the trajectory starts to be deformed, and then a circular trajectory with an inscribed circle appears as shown in the period (C). Thus, the period doubling takes place. It is maintained from the periods (C) to (F). The period doubling has been reported as typical phenomena in nonlinear systems[21]. This is evidence that the secondary mode is induced by nonlinear coupling with the primary mode.

An indication of nonlinear excitation is also observed in growth rate behaviors. Figure 7 shows the amplitude dependence of the growth rate of the secondary mode. After the abrupt jump in the growth rate, the growth rate decreases as the amplitude increases. That is common because the growth of a mode means the consumption of the driving source. After that, once the mode amplitude reaches a threshold value, which is approximately the amplitude of 2 μT under this experimental condition, the growth rate becomes an increasing function of amplitude. This fact indicates that the nonlinear process plays an important role in the mode excitation. A candidate mechanism is proposed in Ref. [20], in which a subcritical instability is shown to be driven by a cooperative collaboration of fluid nonlinearity and kinetic nonlinearity.

The importance of this experimental finding of the abrupt onset of the secondary mode is highlighted from two aspects. First, as is reported in [22, 8, 23], the response of mean ions is stronger as the amplitude of the GAMs increases. A one-half frequency means a one-half phase velocity, and the lower phase velocity will lead to stronger coupling between the mode and thermal ions. The mechanism that causes the onset of the secondary mode is influential for the energy balance of main ions in collisionless plasmas (as in the case of future burning plasmas). The second aspect is the understanding of the 'triggering problem'[18, 19]. The sudden increase in growth rate has been widely observed, and the modeling based on the subcritical instability has been proposed as a working hypothesis[18]. This observation (together with analysis by nonlinear simulation[20]) strongly suggests that the nonlinear excitation mechanisms work, not only in the fluid-like interaction but also in the phase space-nonlinearity. The result identifies an experimental path to study the long-lasting mystery of the triggering problem.

The authors thank Dr. Y. Kosuga and Dr. N. Yokoi for useful discussions and the LHD Technical Group for its support. This work was supported by MEXT Japan under Grant-in-Aid for Scientific Research (A) (No. 15H02155), (C) (No. 24561031, 15K06653), for Challenging Exploratory Research (No. 24656561, 23360414), for Young Scientists (B) (No. 15K18305), NIFS/NINS under NIFS10ULHH020, and the Collaborative Research Program of Research Institute for Applied Mechanics, Kyushu University.

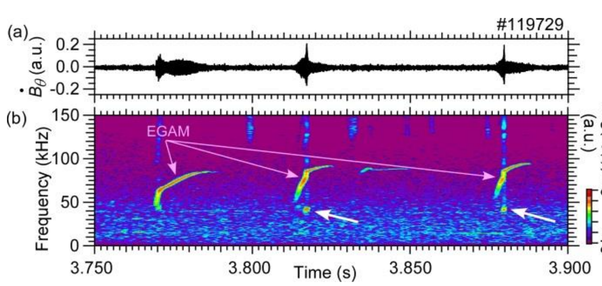

FIG. 1 (a) Typical waveform of a Mirnov signal ($\dot{B}_\theta$), and (b) its spectrogram.

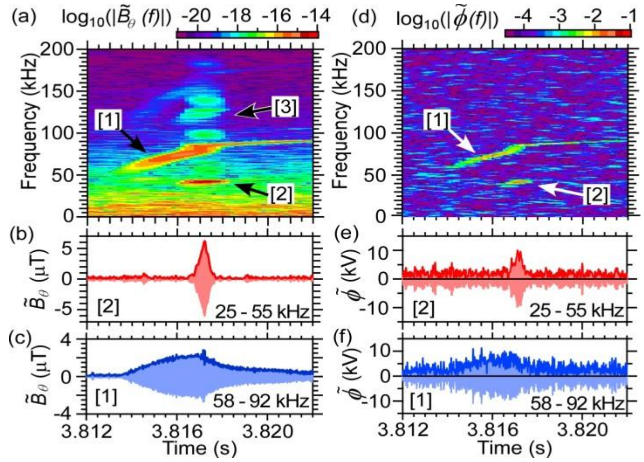

FIG. 2 Top ((a) and (d)): Expanded view of spectrograms of $\tilde{B}_\theta$ and $\tilde{\phi}$. [1], [2], and [3] correspond to the primary mode, the secondary mode, and the mode with a frequency three times the GAM frequency. The measurement position of $\tilde{\phi}$ is at a normalized minor radius of 0.1. Middle and bottom: Waveforms extracted by numerical band-pass filters with the pass band of 25 – 55 kHz ((b) and (e)) and 58 – 92 kHz ((c) and (f)), respectively. Bold curves show the envelopes.

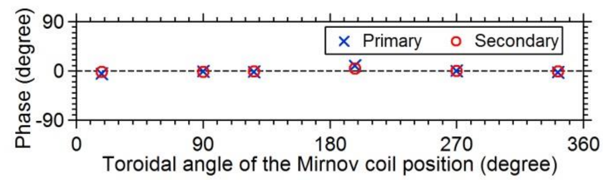

FIG. 3 Phase of $\tilde{B}_\theta$. The horizontal axis is the toroidal angle of the Mirnov coils position, and the reference of the phase is $\tilde{B}_\theta$ at the toroidal angle of 270 degrees.

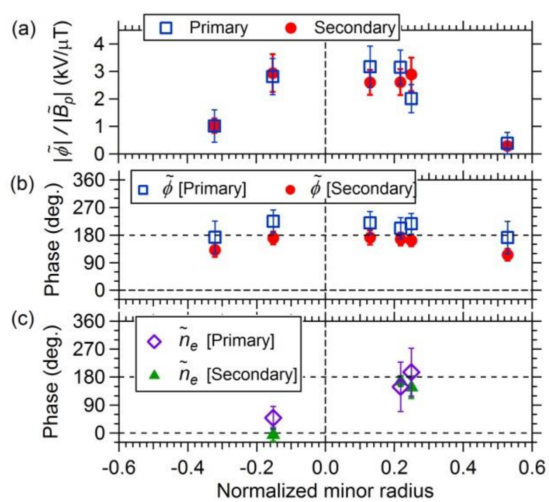

FIG. 4 Radial profiles of (a) amplitude of $\tilde{\phi}$, (b) its phase, and (c) the phase of the HIBP signal intensity which reflects $\tilde{n}$ of the plasma. The amplitudes are normalized by that of $\tilde{B}_\theta$ measured by a Mirnov coil in order to reduce scattering due to differences in experimental conditions. The amplitude of $\tilde{B}_\theta$ ranges from 1.5 to 2 μT for the secondary mode and from 0.7 to 1.2 μT for the primary EGAM. The reference of the phase is $\dot{B}_\theta$. The phases of $\tilde{n}$ at other positions are not plotted because $\tilde{n}$ is too weak at these positions for the phase analysis.

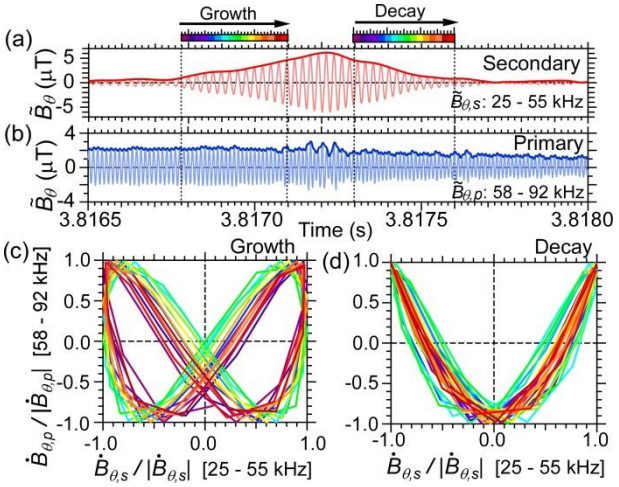

FIG. 5 (a) and (b): $\tilde{B}_\theta$ associated with the secondary mode and the primary mode, respectively. The bold curves show the envelopes. (c) and (d): Lissajous curves between $\dot{B}_\theta$ associated with the secondary mode and the primary mode. (c) and (d) correspond to the growth period and decay period, respectively. The color indicates the time, and the corresponding color bars are plotted above (a).

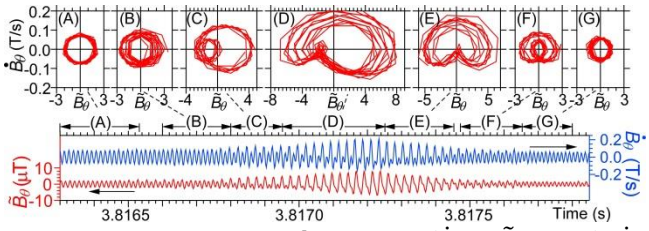

FIG. 6 Trajectories in phase space ($\dot{B}_\theta - \tilde{B}_\theta$ space). $\dot{B}_\theta$ and $\tilde{B}_\theta$ associated with the secondary mode and primary mode are extracted by numerical filters with the pass bands of 25 – 55 kHz and 58 – 92 kHz, as shown in the bottom panel.

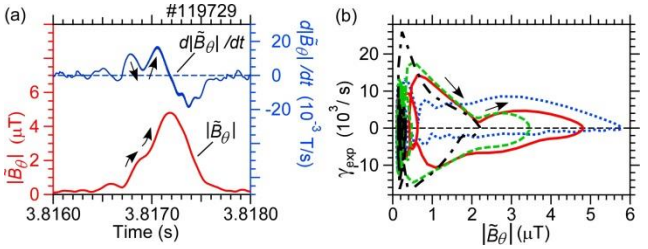

FIG. 7 Growth rate of the magnetic field fluctuation associated with the secondary mode. (a): A typical temporal evolution of the amplitude ($|\tilde{B}_\theta|$) and its time derivative. (b): Amplitude dependence of the growth rate estimated as $\gamma_{exp} = (d|\tilde{B}_\theta|/dt)/|\tilde{B}_\theta|$. Four bursts are plotted.

*Corresponding author: ido@LHD.nifs.ac.jp

[1] P. H. Diamond, S.-I. Itoh, K. Itoh, and T. Hahm, Plasma Phys. Control. Fusion **47**, R35 (2005).
[2] N. Winsor, J. L. Johnson, and J. M. Dawson, Phys. Fluids **11**, 2448 (1968).
[3] K. Hallatschek and D. Biskamp, Phys. Rev. Lett. **86**, 1223 (2001).
[4] Y. Nagashima et al., Phys. Rev. Lett. **95**, 095002 (2005).
[5] H. Berk et al., Nucl. Fusion **46**, S888 (2006).
[6] G. Fu, Phys. Rev. Lett. **101**, 185002 (2008).
[7] R. Nazikian et al., Phys. Rev. Lett. **101**, 185001 (2008).
[8] M. Osakabe et al., Proc. of the 25th IAEA Fusion Energy Conference , Ex/10 (2014).
[9] M. Sasaki, K. Itoh, and S. Itoh, Plasma Phys. Control. Fusion **53**, 085017 (2011).
[10] D. Zarzoso et al., Phys. Rev. Lett. **110**, 125002 (2013).
[11] C. Boswell et al., Phys. Rev. A **358**, 154 (2006).
[12] W. Chen et al., Phys. Lett. A **377**, 387 (2013).
[13] K. Toi et al., Phys. Rev. Lett. **105**, 145003 (2010).
[14] T. Ido et al., Nucl. Fusion **51**, 073046 (2011).
[15] T. Ido et al., Nucl. Fusion **55**, 083024 (2015).
[16] H. Berk, B. Breizman, and N. Petviashvili, Phys. Lett. A **234**, 213 (1997).
[17] M. Lesur and Y. Idomura, Nucl. Fusion **52**, 094004 (2012).
[18] S. Itoh, K. Itoh, H. Zushi, and A. Fukuyama, Plasma Phys. Control. Fusion **40**, 879 (1998).
[19] A. Bhattacharjee, Z. W. Ma, and X. Wang, *Lecture Notes in Physics 614: Turbulence and Magnetic Fields in Astrophysics*, Springer, Berlin, 2003.
[20] M. Lesur et al., submitted to Phys. Rev. Lett. (2015).
[21] T. Klinger et al., Phys. Plasma **8**, 1961 (2001).
[22] T. Ido et al., Proc. of the 24th IAEA fusion energy conference **PD/P8-16** (2012).
[23] K. Ida et al., Nucl. Fusion **55**, 104018 (2015).